Article:
Yao, X, Zhang, Y, Lu, C et al. (1 more author) (2016) CFD investigation of gas-solids flow in a new fluidized catalyst cooler. Powder Technology, 304. pp. 108-119. ISSN 0032-5910

https://doi.org/10.1016/j.powtec.2016.08.022

CFD investigation of gas-solids flow in a new fluidized catalyst cooler

Xiuying Yao[a,b], Yongmin Zhang[a,*], Chunxi Lu[a,*], Dongsheng Wen[b,*]

[a] State Key Laboratory of Heavy Oil Processing, China University of Petroleum, Beijing 102249, P.R. China

[b] School of Chemical and Process Engineering, University of Leeds, Leeds LS2 9JT, UK

* Corresponding authors. E-mail addresses: zym0876@gmail.com (Y. Zhang), lcx725@sina.com (C. Lu) or d.wen@leeds.ac.uk (D. Wen)

Abstract: In our previous work, a new concept of annular catalyst cooler (ACC) was recently proposed and validated experimentally, which showed that an internal circulation of solids can be formed by using two gas distributors and both hydrodynamics and heat transfer can be largely improved. The current work simulated the detailed hydrodynamics of gas-solids flow to advance our understanding of the ACC by using the two-fluid model.. The influence of effective particle diameter d_p^* and specularity coefficient φ in solids wall boundary condition are examined and compared with experimental data. Optimum values of d_p^*=170 μm and φ=0.3 are determined and used in the simulations. The results show that by properly selecting the gas velocities and the position of heat transfer tube, internal solids circulation can be formed. TheACC has a combined hydrodynamic feature of up- and down-flow catalyst coolers with bigger solids volume fraction and smaller particle resident time, which are beneficial for improving heat transfer coefficients. Detailed hydrodynamics of gas-solids flow are obtained, and the influential parameters are examined, which provides valuable information on the design and optimization of such new ACCs.

Keywords: internal circulation, hydrodynamics, gas-solid flow, catalyst cooler, FCC, CFD

1. INTRODUCTION

In a modern petroleum refinery, a catalyst cooler plays a crucial role to keep heat balance of a fluid catalytic cracking (FCC) unit for processing heavy residue feedstock [1, 2]. A heat balance is achieved when the generated heat from the coke-burning regeneration is equal to the required heat for the cracking reaction. However for high coke-contained feedstock, the heat released is generally much more than the requirement from the cracking reaction. Such extra heat leads to a reduction in processing capacity with worsened product yields or even serious accidents [3, 4]. The catalyst cooler is a surface type heat exchanger, where the heat is transferred from hot particles to a bundle of tubes and taken away by water and stream inside. Both down-flow and up-flow external catalyst coolers are widely used in the actual industry [4,5]. .

However when feedstocks become heavier and poorer in quality, it is difficult for conventional external catalyst coolers to meet the industrial demand [4, 6-8]. Several problems such as low heat transfer capacity, unstable catalyst circulation and severe tube damages were frequently reported in industrial catalyst coolers [9-11]. In our previous studies, a new catalyst cooler (ACC) concept based on annular flow configuration was proposed to intensify the bed-to-wall heat transfer and improve the hydrodynamics of gas-solids flow [12]. In this new concept, the single gas distributor associated with conventional catalytic coolers was replaced by two distributors, including a centre plate distributor and a ring distributor near the bed wall. An internal particle circulation motion can be formed by adjusting the ratios of gas velocities from two gas distributors. Our experiments have validated the new concept of ACC and showed that the internal circulation of solids played a dominant role in improving the hydrodynamics of gas and solids flow, and enhancing particles renewal on the tube surface [13]. Further comparison of the flow and heat transfer behaviour against a base catalyst cooler (BCC) showed the promise of the new ACC concept.

However, it shall be noted that due to the experimental limitations, the detailed hydrodynamics of gas and solids in the critical fluidized regions are still unclear. As summarized in our previous studies [12, 13], the design idea of the ACC was originated from a recirculation fluidized bed (RCFB) [14, 15]. For RCFBs, many studies have been conducted to obtain the profiles of bed density and solids velocity [16, 17], particle residence time distribution [18], particle circulating velocity [19, 20], and cold and hot particle mixing degree [21, 22] in the critical regions. However, an ACC bears significant differences to a RCFB in terms of the double distributor design and system configuration. As small variations in the design may lead to large differences in the performance, it is essential to understand detailed hydrodynamics of gas and solids in an ACC..

Computational Fluid Dynamics (CFD) based on the Euler-Euler method has been successfully applied to investigate the micro-structure of gas and solids flow [22], heat transfer performance and operation optimization of industrial processes [23, 24]. For bed-to-wall heat transfer, most of investigators focused on the predicting ability of the model on the heat transfer coefficient near the hot wall or the effect of bubble movement on heat transfer coefficient. For example, Kuiper et al [25] obtained detailed information on the maximum bed-to-wall heat transfer occurs in the bubble wake by a two fluid model without incorporation of turbulence terms. Patil et al [26] simulated a case with a pulsating jet by incorporating a porosity profile near the wall in the thermal energy balance, based on the effective heat conductivity. And the computed local instantaneous heat-transfer coefficient was in good agreement with the experimentally determined heat-transfer coefficients. Yusuf et al [27] found the better results were predicted by using the model of Legawiec and Ziolkowski [28] rather than Zehner and Schluender [29] to calculate the solid phase thermal conductivity. Moreover, another researches aimed to obtain the relation between the gas-solids hydrodynamics and bed-to-tube heat transfer in a fluidized bed with immersed heated tube. Armstrong et al [30] used a two-fluid Eulerian-Eulerian formulation incorporating the KTGF to simulate the 2D fluidized bed with horizontal heated immersed tubes. Results showed that increasing the number of tubes promoted heat transfer from tubes to the particles and flow. Further, Dong et al [31] found a square heated tube influenced the hydrodynamics more than the circular tube which delayed the bed from reaching fluidization by investigating the effect of tube shape. Yusuf et al [32] simulated the local instantaneous heat transfer coefficient at the top of the tube, which was strongly affected by the gas velocity. All studies reviewed above simulated the hydrodynamics, heat transfer or their relation in the local region near the wall or tube. However, little investigator focuses on the effect of whole gas-solid flow on heat transfer coefficient in a fluidized bed with vertical heated tube. In this study, the gas and solids flow will be simulated to obtain the effect of hydrodynamics on the heat transfer performance on the basic of our pervious experimental measurements [12, 13].

In industrial catalyst cooler, FCC particles, a typical Geldart group A particle, are fluidized by air to form the bubbling fluidized bed. Ferschneider and Mege[33] observed severe overestimation of bed expansion by simulating a freely bubbling bed of FCC particles using an Euler-Euler method. After an extensive review, van Wachem et al [34] found that drag force has a significant impact on the simulation results, influencing the predicted bed expansion and the solids concentration in the dense phase regions of the bed. The poor simulation results for Geldart A particles were attributed to the existence of cohesive inter-particle forces that are due to particle-particle collision. The inter-particle force leads to the grouping of solids or particle clusters, resulting in an effectively larger particle diameter and a lower interphase exchange coefficient, which would in turn led to a reduced bed expansion

[35]. For instance, Mckeen and Pugsley [35] showed that the effective particle agglomerate diameter was in the range of 135~170 μm for FCC particles with an actual mean diameter of 75 μm. Lettieri et al [36] back-calculated the cluster diameters from the experimental terminal velocity, and showed that FCC particles with a Sauter mean diameter from 49 to 71 μm had an effective particle diameter in the range of 200~400 μm at 20 ºC and in the range of 100~117 μm at 650 ºC. Gao et al [37, 38] proposed a modified drag model based on the effective mean diameter of particles cluster, and successfully simulated the gas and solids mixing in FCC strippers [39] and hydrodynamics in a gas-solid airlift loop reactor [18].

As a complementary work to our experimental studies [12,13], the Euler-Euler model is adopted in this work to simulate gas-solids flow in a BCC and an ACC. The effective particle diameters and the specularity coefficient (i.e., to describe particle-wall collision boundary conditions) are obtained by comparing the simulation with experimental data. The drag model modified by Gao et al [37, 38] is used to model the inter-particle force based on the effective particle diameters. A parametric investigation of the operation conditions and optimization are numerically simulated and detailed hydrodynamics is then revealed in the critical flow regions, as well as the driving force of internal circulation, including solids volume fraction, velocity, flux and their standard derivation.

2. MODEL DESCRIPTION

2.1 Numerical model

Numerical modeling of the fluidized bed system was based on the two-fluid model, and the equations for the conservation of mass, momentum and granular temperature were solved by the commercial CFD program FLUENT 6.3.26. The kinetic theory of granular flow, which characterizes the stochastic fluctuations of the kinetic energy of solids, is used for the closure of the solids stress terms. The governing equations solved for the current gas-solids system are as follows:

Mass conservation for the gas and solids phases:

$$\frac{\partial}{\partial t}\left(\varepsilon_g \rho_g\right)+\frac{\partial}{\partial x_j}\left(\varepsilon_g \rho_g u_{gj}\right)=0 \tag{1}$$

$$\frac{\partial}{\partial t}\left(\varepsilon_p \rho_p\right)+\frac{\partial}{\partial x_j}\left(\varepsilon_p \rho_p u_{pj}\right)=0 \tag{2}$$

Momentum conservation for the gas and solids phases:

$$\frac{\partial}{\partial t}\left(\varepsilon_g \rho_g u_{gj}\right)+\frac{\partial}{\partial x_j}\left(\varepsilon_g \rho_g u_{gi} u_{gj}\right)=-\varepsilon_g \frac{\partial p}{\partial x_j}+\frac{\partial \tau_{g,ij}}{\partial x_j}-\beta\left(u_{gi}-u_{pi}\right)+\varepsilon_g \rho_g g_i \tag{3}$$

$$\frac{\partial}{\partial t}\left(\varepsilon_p \rho_p u_{pj}\right)+\frac{\partial}{\partial x_j}\left(\varepsilon_p \rho_p u_{pi} u_{pj}\right)=-\varepsilon_p \frac{\partial p}{\partial x_j}+\frac{\partial \tau_{p,ij}}{\partial x_j}-\beta\left(u_{pi}-u_{gi}\right)+\varepsilon_p \rho_p g_i \tag{4}$$

Here ε is the volume fraction, ρ is the density, u is the velocity, t is the time, p is the pressure, g_i is the gravity acceleration and β is the interphase momentum exchange coefficient, respectively. The subscripts g and p indicate the gas and particle phases.

The conservation of the kinetic energy of the moving particles is described by the granular temperature, Θ, which is derived from the kinetic theory of granular flow:

$$\frac{3}{2}\left[\frac{\partial}{\partial t}\left(\varepsilon_p \rho_p \Theta\right)+\frac{\partial}{\partial x_k}\left(\varepsilon_p \rho_p u_{pk} \Theta\right)\right]=\frac{\partial}{\partial x_k}\left(\Gamma_\Theta \frac{\partial \Theta}{\partial x_k}\right)+\mu_p\left(\frac{\partial u_{pk}}{\partial x_i}+\frac{\partial u_{pi}}{\partial x_k}\right)\frac{\partial u_{pk}}{\partial x_i} - p_p \frac{\partial u_{pk}}{\partial x_k}+\left(\xi_p-\frac{2}{3}\mu_p\right)\left(\frac{\partial u_{pk}}{\partial x_k}\right)^2-\gamma \tag{5}$$

where Θ is the granular temperature, Γ_Θ is the diffusion coefficient, μ_p is the solid phase shear viscosity, p_p is the solid phase pressure, ξ_p is the solid bulk viscosity, and γ is the collisional dissipation of solid fluctuating kinetic energy.

Due to several unknown variables included to the kinetic theory of granular flow, constitutive equations are needed to close the conservation equations, as below.

The stress tensor for the gas phase is described as:

$$\tau_{g,ij}=\mu_g\left(\frac{\partial u_{gj}}{\partial x_i}+\frac{\partial u_{gi}}{\partial x_j}\right) \tag{6}$$

while the stress tensor for the solids phase is:

$$\tau_{p,ij}=\mu_p\left(\frac{\partial u_{pj}}{\partial x_i}+\frac{\partial u_{pi}}{\partial x_j}\right)+\left(\xi_p-\frac{2}{3}\mu_p\right)\frac{\partial u_{pk}}{\partial x_k}\delta_{ij}-p_p\delta_{ij} \tag{7}$$

The solid phase pressure, which describes the change in the total momentum transport of the motion of particles and their interactions, is used for the pressure gradient term and is expressed as:

$$p_p=\varepsilon_p \rho_p \Theta\left[1+2g_0\varepsilon_p\left(1+e\right)\right] \tag{8}$$

where e is the particle-particle restitution coefficient, and g_0, the radial distribution function, is expressed as:

$$g_0=\left[1-\left(\varepsilon_p/\varepsilon_{p,max}\right)^{1/3}\right]^{-1} \tag{9}$$

The granular temperature is defined by:

$$\Theta=\frac{1}{3}\left\langle \overline{u_p' u_p'} \right\rangle \tag{10}$$

The solid phase shear viscosity is determined by:

$$\mu_p = \frac{10\rho_p d_p\sqrt{\pi\Theta}}{96(1+e)g_0}\left[1+\frac{4}{5}(1+e)g_0\varepsilon_p\right]^2 + \frac{4}{5}\varepsilon_p^2\rho_p d_p g_0(1+e)\sqrt{\frac{\Theta}{\pi}} \tag{11}$$

The solids bulk viscosity, which accounts for the resistance of the solid phase to compression and expansion, is expressed by:

$$\xi_p = \frac{4}{3}\varepsilon_p\rho_p d_p g_0(1+e)\sqrt{\frac{\Theta}{\pi}} \tag{12}$$

The collision dissipation of energy, representing the rate of energy dissipation in the particulate phase due to inelastic particle collisions, is calculated by:

$$\gamma = 3(1-e^2)\varepsilon_p^2\rho_p g_0\Theta\left[\frac{4}{d_p}\sqrt{\frac{\Theta}{\pi}} - \frac{\partial u_{pk}}{\partial x_k}\right] \tag{13}$$

The conductivity of the solid fluctuating kinetic energy describes the diffusion of granular energy as:

$$\Gamma_\Theta = \frac{150\rho_p d_p\sqrt{\pi\Theta}}{384(1+e)g_0}\left[1+\frac{6}{5}(1+e)g_0\varepsilon_p\right]^2 + 2\varepsilon_p^2\rho_p d_p g_0(1+e)\sqrt{\frac{\Theta}{\pi}} \tag{14}$$

The exchange coefficient β in Eq. (3) and (4) is used to couple the drag interaction between the gas and solids phases. Due to the strong inter-particle force between Geldart A type particles, a grouping of solids or particle clusters occur in the fluidized system where many studies have been conducted [37, 38, 40]. The modified Gidaspow drag model by Gao et al [37] is used in this work to compute the drag force of formed agglomerates.

$$\beta = 150\frac{\varepsilon_p(1-\varepsilon_g)\mu_g}{\varepsilon_g(d_p^*)^2} + 1.75\frac{\rho_g\varepsilon_p|\vec{u}_p-\vec{u}_g|}{d_p^*} \qquad \varepsilon_g \le 0.8 \tag{15}$$

$$\beta = \frac{3}{4}C_D\frac{\varepsilon_p\varepsilon_g\rho_g|\vec{u}_p-\vec{u}_g|}{d_p^*}\varepsilon_g^{-2.65} \qquad \varepsilon_g > 0.8 \tag{16}$$

$$C_D = \begin{cases}\dfrac{24}{Re_p}(1+0.15Re_p^{0.687}) & (Re_p \le 1000)\\ 0.44 & (Re_p > 1000)\end{cases} \tag{17}$$

$$Re_p = \frac{\varepsilon_g\rho_g d_p^*|\vec{u}_g-\vec{u}_p|}{\mu_g} \tag{18}$$

where d_p* is the effective particle diameter, C_D is the drag coefficient, μ_g is the viscosity of gas, and Re_p is the Reynolds number of agglomerate.

2.2. Simulation system

Numerical simulation was performed under the same conditions as the

experimental work described in our previous paper [13]. As shown in Figure 1, the experimental facilities were simplified to a two-dimensional structure with the height 0.3 m and width of 0.286 m. The heat transfer tube had a height of 0.844 m and width of 0.04 m. The fluidized bed was divided into two regions by the tube. One was the region closing to the bed center, which was simply named as the 'left region' according to their relative positions. Another was the region closing to the bed wall, named as the 'right region'. In order to obtain a uniform rectangular mesh, the inlet was simplified as the uniform velocity inlet, and mesh size of 4 mm*4 mm was used. The entrained particles from the top outlet were returned to the bed from the bottom inlet by a user defined function.

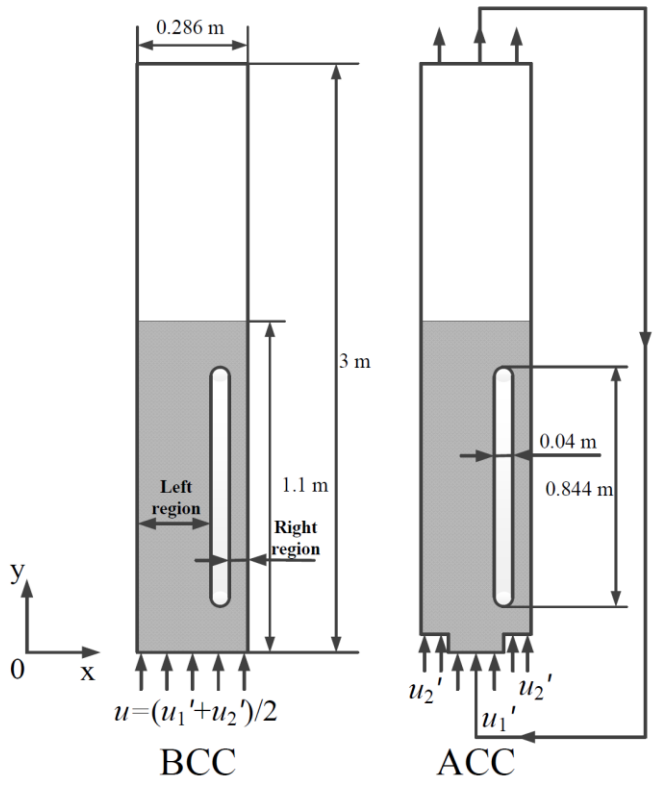

Figure 1 Schematic diagram of simulated 2D fluidized bed catalyst coolers

Table 1 Gas and particle properties and operation conditions

Item	Value
Particle diameter, d_p	69.4 μm
Particle density, ρ_p	1500 kg/m^3
Minimum fluidization velocity, u_{mf}	0.0035 m/s
Air density, ρ_g	1.225 kg/m^3
Air viscosity, μ_g	1.7 ×10^{-5} kg/(m·s)
Inlet gas velocity	
Form distributor in BCC, u	0.1, 0.2, 0.3, 0.4, 0.5 m/s

Form plate distributor in ACC, u_1'	0.17, 0.37, 0.57, 0.77, 0.97 m/s
Form ring distributor in ACC, u_2'	0.03 m/s
Radial position of heat tube, r/R_w	0, 0.3, 0.6, 0.8, 0.9, 0.95
Static bed height, H_0	1.1 m
Initial solids volume fraction, ε_0	0.55
Specularity coefficient, φ	0.05, 0.2, 0.3, 0.35, 0.5, 0.9
Particle coefficient of restitution, e	0.9
Wall coefficient of restitution, e_w	0.9

The gas used was air at ambient conditions and the particles were FCC catalysts. The properties of gas and particle and the corresponding experimental conditions are listed in Table 1. All inlets were designated as velocity inlet boundary condition, where their flow directions were normal to the boundary. Based on the experiment, the inlet velocity of gas phase was determined from the superficial gas velocity, and the inlet velocity of solids phase was zero due to no solids flow into the bed. As the flow area was the same as that in the BCC, the inlet velocity was equal to the superficial gas velocity, in the range of 0.1~0.5 m/s. However, the area of each distributor was equal to half of the bed cross sectional area in the ACC, i.e.

$$A_1 = A_2 = \frac{1}{2} A \tag{19}$$

where A, A_1 and A_2 were the bed cross sectional area, the areas of plate distributor and ring distributor, respectively. Based on the continuity principle, there is a relation between the inlet velocities from the centre plate distributor u_1', from the ring distributor u_2', and superficial gas velocity u,

$$uA = u_1' A_1 + u_2' A_2 \tag{20}$$

During the experiments, two catalyst coolers were kept at same superficial gas velocities. Therefore, u_1' was in a range of 0.17~0.97 m/s when u_2' was fixed at 0.03m/s. The top of the bed was set as the pressure outlet boundary condition for the two phases. At the wall, a no-slip boundary condition was assumed for the gas phase. For the solids phase, the Johnson and Jackson [41] solid phase wall boundary condition was adopted to describe the interactions between particles and wall. The equations for boundary conditions used are given in Table 2. The specularity coefficient φ is an empirical parameter describing the particle-wall collisions. Its value has a range from zero for perfect specular collision to unity for perfect diffuse collision [42]. A smaller value generally represents a smooth wall with less friction. The specularity coefficient was set as 0.05, 0.2, 0.3, 0.35, 0.5 and 0.9 to investigate their effect on the gas-solids flow. No- and free-slip boundary conditions also were considered to investigate the effect of wall boundary condition, corresponding to φ=1 and 0. Both the particle coefficient of restitution and the wall coefficient of restitution were set to 0.9. Initially, the catalyst cooler was filled with FCC particles at an appropriate initial volume

fraction (0.55). At initial state, the particle velocity and the bed height were set as the minimum fluidizing velocity 0.0035 m/s and 1.1 m, respectively. The time step used was 0.001s. Both the time step and mesh size were tested for independence. The fluidized bed achieved a steady state for a period of 10 s.

During the actual experiment [13], the radial average of solids volume fraction and instantaneous solids volume fraction on the tube surface were measured to obtain the bed expansion ratio and the surface hydrodynamics in the BCC, which are used to validate the model. In addition, the bed-to-tube heat transfer coefficients were measured by a heated tube and thermocouples in the BCC and ACC, and will be used to illustrate the influence of hydrodynamics via the modelling. Please refer to our paper for detailed experimental description [13].

Table 2 Johnson and Jackson [41] solids wall boundary conditions

Item	Expression
Velocity	$u_{s,w} = -\frac{6\mu_s\varepsilon_{s,max}}{\sqrt{3}\pi\varphi\rho_s\varepsilon_s g_{0,ss}\sqrt{\Theta_s}}\frac{\partial u_{s,w}}{\partial n}$
Granular temperature	$\Theta_w = -\frac{k_{\Theta_s}}{\gamma_w}\frac{\partial\Theta_w}{\partial n} + \frac{\sqrt{3}\pi\varphi\rho_s\varepsilon_s u_{s,slip}^2 g_{0,ss}\Theta_s^{3/2}}{6\varepsilon_{s,max}\gamma_w}$
	$\gamma_w = \frac{\sqrt{3}\pi\left(1-e_w^2\right)\varepsilon_s\rho_s g_{0,ss}\Theta_s^{3/2}}{4\varepsilon_{s,max}}$

3. PARAMETERS DETERMINATION

3.1 Effective particle diameter

The effective particle diameter d_p* is of crucial importance to the modified Gidaspow drag model. It directly influents whether the predicted bed expansion ratio is in agreement with experimental value or not [18]. In the simulation, the effective particle diameter is set as 69.4 μm, 170 μm, 250 μm, 300 μm and 400 μm respectively to determine the appropriate particle cluster diameter. For axial distribution of solids volume fraction, the simulated values are compared with the experimental ones from the BCC at u=0.3 m/s, Figure 2. The predicted particle volume fraction and bed expansion height are in good agreement with the measured values when the d_p* is equal to 170 μm. For the smaller effective particle diameter 69.4 μm, the calculation gives a severe over-prediction of the experimental bed expansion. For the bigger effective particle size, i.e. 250 - 400 μm, larger solids volume fractions are obtained due to smaller drag force and correspondingly, a smaller bed expansion height. So the

effective particle diameter 170 μm is selected in this work to simulate the gas and particles hydrodynamics in two catalyst coolers.

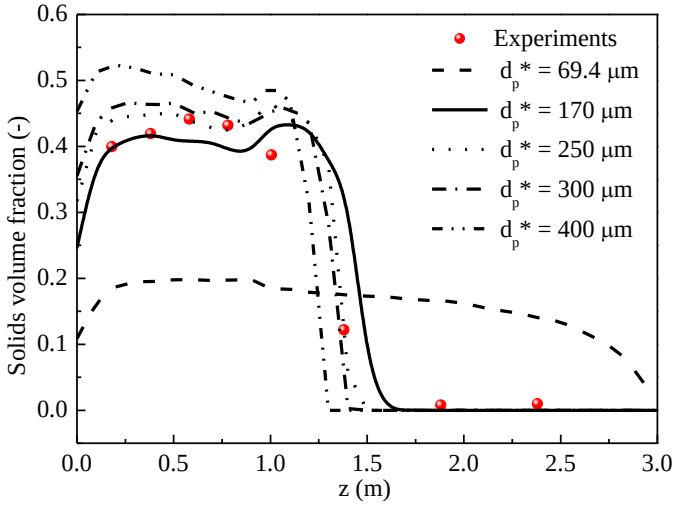

Figure 2 Effect of the effective particle diameter on solids volume fraction distribution (u=0.3 m/s, φ=0.3, e_w=0.9)

3.2 Specularity coefficient

Zero, partial- and free-slip wall-boundary conditions are respectively used to investigate the effect of particle-wall interactions. The partial-slip wall boundary condition proposed by Johnson and Jackson [41] includes two important parameters to describe the fluctuating energy due to the inelastic collision between particles and wall, and the tangential particles velocity at the wall. The fluctuating energy is specified by the particle-wall restitution coefficient (e_w). Another parameter is the specularity coefficient (φ), which characterizes the sliding and bouncing back behaviours of particles [42]. For both 2D and 3D bubbling fluidized beds, the simulation results from Li et al [43] has shown that the restitution coefficient had a smaller influence on the radial profiles of solids volume fraction and velocity, but the specularity coefficient influenced gas and solids flow significantly. Zhong et al [44] also found that the restitution coefficient played only a minor role in predicting the segregation and mixing behaviour of binary particle mixtures in a bubbling bed. However, for both segregation and mixing process, the specularity coefficient significantly affected the predicted jetsam velocity distributions, which was obviously different in terms of jetsam concentration distribution. The same results were also obtained in in spouted beds [45]. In this study, the particle-wall restitution coefficient 0.9, which was employed in many studies [46,47], was used and the effect of specularity was examined corresponding to different boundary conditions.. In the study, a free-slip boundary condition is simulated with φ=0, and the no-slip boundary condition is represented by φ=1, similar to previous studies [49-51]. In the partial-slip

boundary condition, the specularity coefficient is set as 0.05, 0.2, 0.3, 0.35, 0.5 and 0.9.

Figure 3 presents the axial profiles of solids volume fraction at different wall boundary conditions, which shows that the influence of the specularity coefficient is small. Except the free-slip case (φ=0) where a peak value is observed at z=1 m, all other simulations reach similar results and are in good agreement with the experimental values. Such results are consistent with Loha et al [48] who found the predicted pressure drop across the bed was also similar except for the free-slip condition, which showed the maximum deviation. .

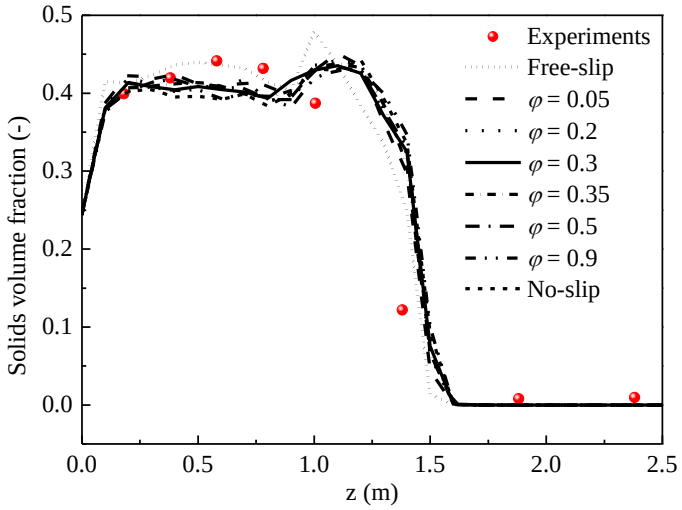

Figure 3 Effect of specularity coefficient on solids volume fraction in the axial direction (u=0.3 m/s, d_p*=170 μm and e_w=0.9)

Though the influence of the specularity coefficient on the average solid volume fraction is small, the simulation results from Li et al [43] and Loha et al [48] showed that the specularity coefficient would affect the radial distribution of solid volume fraction. Experimentally, we have developed an optical fibre probe to monitor the transient solids flow near the wall. When the particles or bubbles flow through the heat transfer tube, the voltage signals measured by the probe will fluctuate correspondingly, which indicates the change of the solids volume fraction. Figure 4 compares the simulated instantaneous solids volume fractions with the experimental values at z=0.5 m at different wall boundary conditions. As the shear effect of the wall on the particles decreases with reducing specularity coefficient, the particles tends to reside at the wall region at the low specularity coefficient [52,53]. The smaller specularity coefficient would cause lower frequency of bubbles occurred at the wall, forming bigger solids volume fraction. It is found that the simulation value for φ=0.3 is closer to the experimental value. Therefore, the specularity coefficient 0.3, which is very close to φ= 0.25 used by Armstrong et al [30,54], for the partial-slip boundary condition is selected to simulate the flow of gas and particles in two catalyst coolers. The selected specularity value is also consistent with the recommendations from Bakshi et al[55],

who suggested that values of φ shall be n the range of [0.01, 0.3] to simulate dense solid-gas flows.

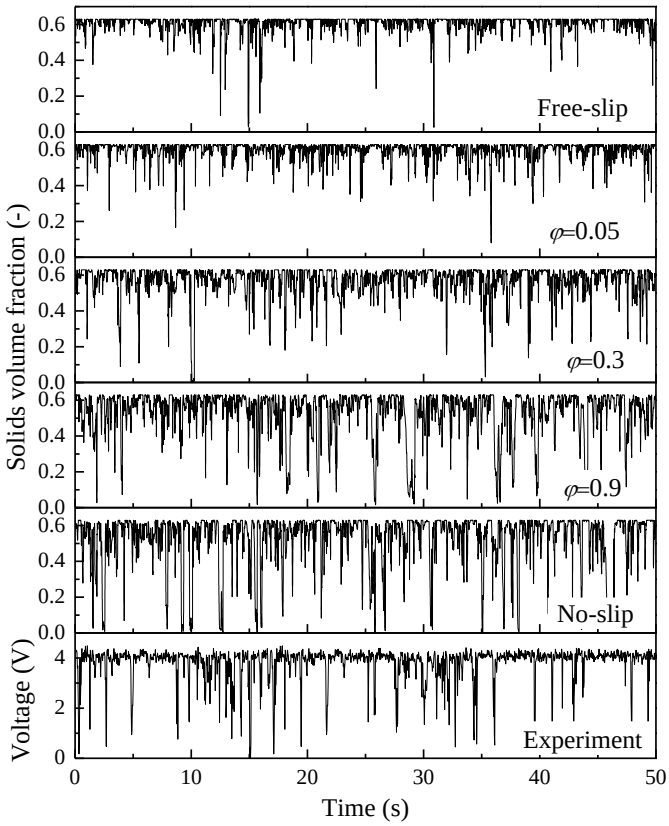

Figure 4 Effect of specularity coefficient on instantaneous solids volume fraction （z=0.5 m）

4. RESULTS AND DISCUSSION

Based on experimentally-validated effective particle dimeter and specularity coefficient, extensive simulation is conducted to reveal detailed hydrodynamics of the gas and solid phase and the influence of the operational conditions, as described below.

4.1 Particle radial distribution

Figure 5(a)~(f) respectively compare the radial distribution of solids volume fraction and velocity in the BCC and ACC when the heat tube is fixed at r/R_w=0, 0.3, 0.6, 0.8, 0.9, 0.95 for a given superficial gas velocity of 0.3 m/s at z=0.5 m, where r is the distance between tube centre and bed centre and R_w is the maximum radial position that the heat transfer tube can reach, i.e., bed radius R minus the tube radius r_t. The BCC has clear characteristics of a bubbling bed, which is not influenced by the radial position of heat tube due to uniform gas distribution. The particles ascend in the centre region and descend near the wall, resulting in a smaller solids volume fraction in the centre region and a higher value toward the bed wall or tube wall.

When the heat tube is fixed in the bed centre, i.e., r/R_w =0.0, the ACC has similar flow state and solids distribution as the BCC due to the symmetry of the flow region. The distribution is not changed with time, as shown in Figure 6(a). Such a result is consistent with the experimentally determined heat transfer coefficient trend, where nearly identical values were obtained in the BCC and ACC at the bed centre, as shown in Figure 7[13]. Although there is asymmetrical gas distribution at r/R_w =0.3, a complete internal circulation is not achieved. According to the change of solids volume fraction with time in Figure 6(b), there is an unsteady solids internal circulation in the ACC. This unsteady flow state is attributed to smaller difference of gas velocity and circulation area between the two regions. Correspondently the improvement of heat transfer performance is limited in the ACC at r/R_w =0.3.

When the heat tube is close to the bed wall, i.e., r/R_w>0.6, the ACC presents a different flow state from the BCC, where the particles move upward in the left region and downward in the right region. The particles form a steady internal circulation in the ACC, not changing with time (as shown in Figure 6(c) and (d)), which is reflected in the salient increase in the heat transfer coefficient, Figure 7. When the heat tube is installed at r/R_w=0.6 and 0.8, the ACC has larger solids velocity than that of BCC in the left region, although their solids volume fractions have the same profiles. At r/R_w=0.6, the heat transfer coefficient in the ACC reaches the maximum value, i.e., 550 W/Km^2, a 22% increase over the BCC. When fixing the heat tube at r/R_w=0.9 and 0.95, both solids volume fraction and velocity in two catalyst coolers show identical radial profiles in the left region. In their right regions, the solids volume fraction of the ACC is always bigger than that of the BCC. By comparing the solids velocity, it is found that the solids internal circulation rate at r/R_w=0.6 and 0.8 is bigger than the ones at r/R_w=0.9 and 0.95. Correspondingly, the heat transfer coefficient is also bigger. It is expected that both the smaller circulation area and the stronger shear effect from the wall limit the movement downward of solids in the right region at higher r/R_w values.

Such results show that the particles in the left region have the characteristics of a bubbling fluidization with a high velocity, which is similar to those of an up-flow catalyst cooler. The right region is a bubbling fluidization with a low velocity and has similarities with a down-flow catalyst cooler. Consequently, the ACC has a combined hydrodynamic behavior of both up-flow and down-flow catalyst coolers.

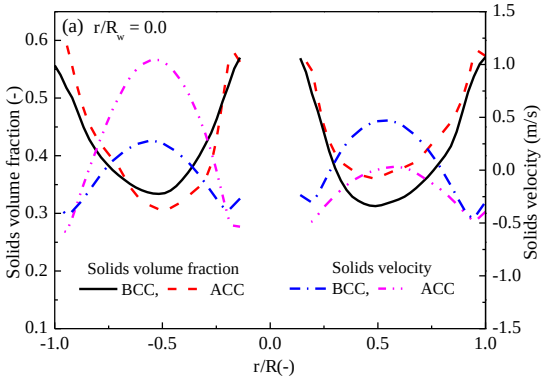

(a) r/R_w=0

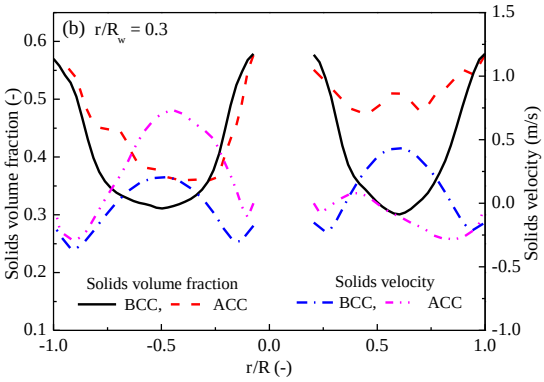

(b) r/R_w=0.3

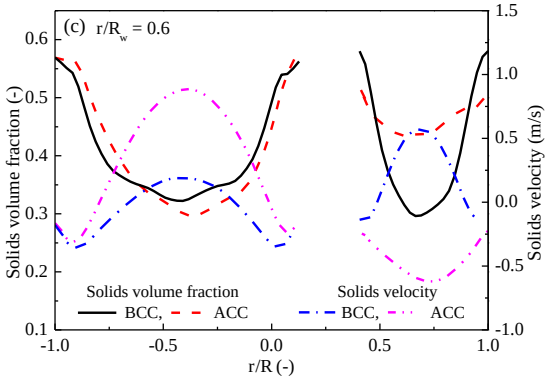

(a) r/R_w=0.6

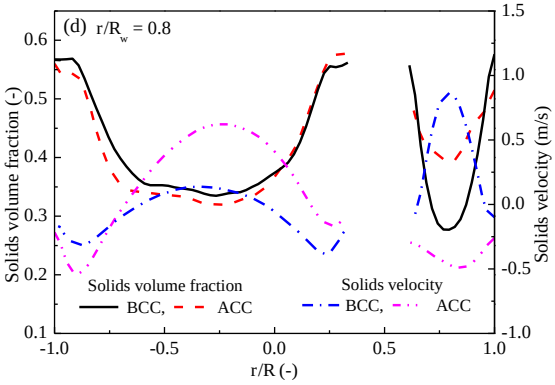

(b) r/R_w=0.8

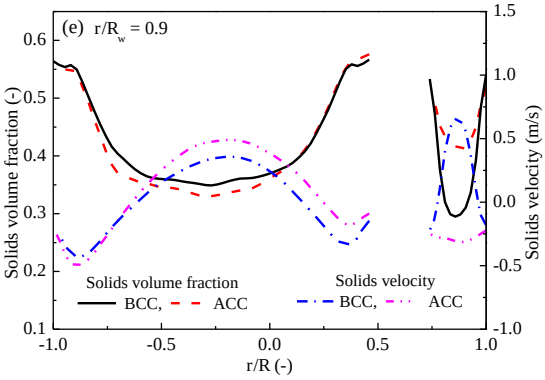

(a) r/R_w=0.9

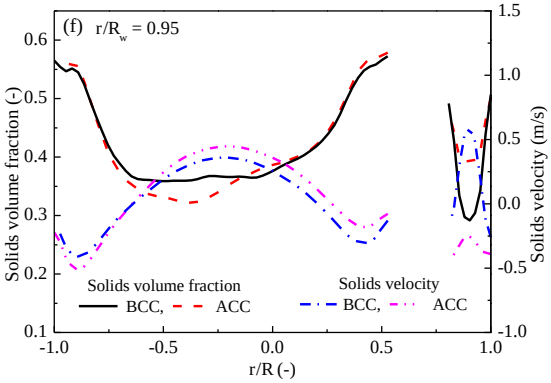

(b) r/R_w=0.95

Figure 5 Comparison of solids volume fraction and velocity in two catalyst coolers

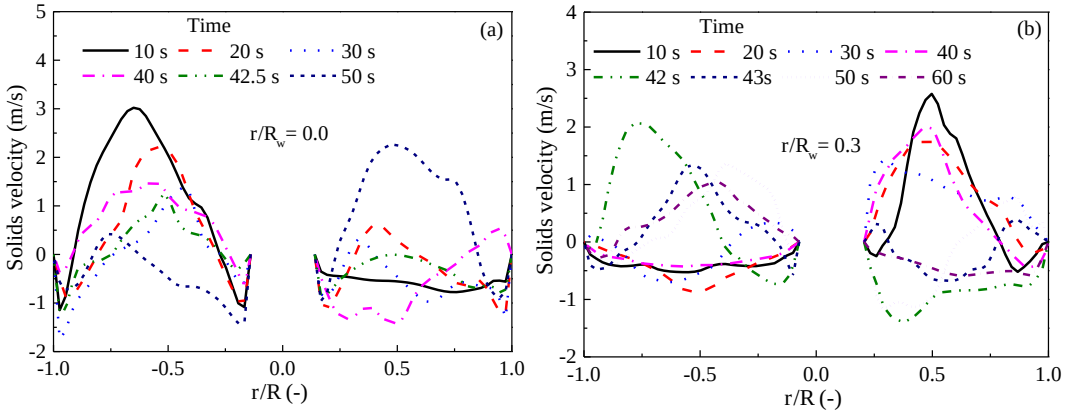

(a) r/R_w=0 (b) r/R_w=0.3

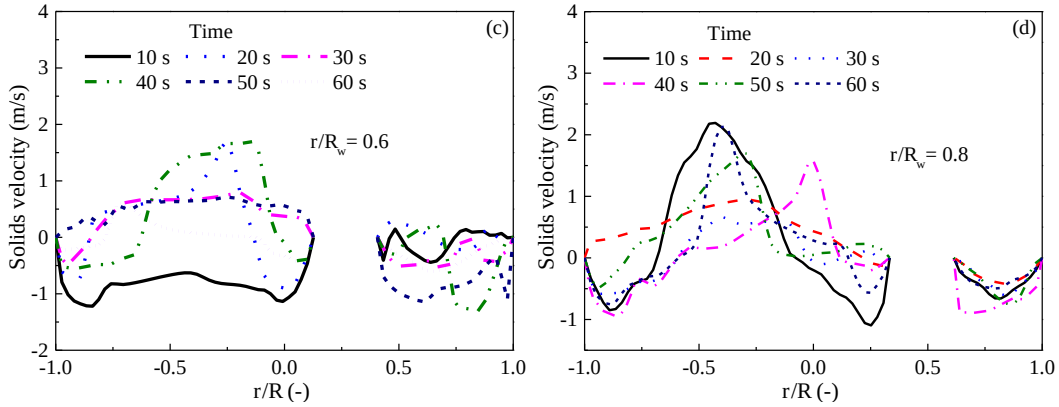

(a) r/R_w=0.6 (b) r/R_w=0.8

Figure 6 Change of solids velocity with the time in the ACC

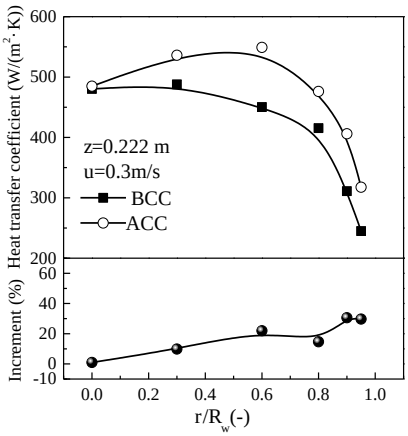

Figure 7 Improvement of heat transfer coefficient at u=0.3 m/s [13]

4.2 Axial distribution

Figure 8 shows examples of the instantaneous solids flux in two sides of the heat tube at u=0.3 m/s and r/R_w=0.8. Here the solids flux is an area-averaged value based on the flow area of each side [56]. It presents a great periodicity in the left region of BCC. There is a high frequency for particles movement upward and downward, with

similar amplitudes of fluctuations. In the right region, the solids flux is bigger than that in the left region, i.e., almost doubled as shown in Figure 8(a). This is attributed to the presence of bigger bubbles flowing through the right region, where the bubble size approximately equals to the flow area as shown in Figure 9(a). But their time-averaged values are very close due to continuous particles descending for several seconds. The fluctuating curves show a back-mixing motion in the BCC, which are typical characteristics of a bubbling bed.

The ACC has similar frequency and amplitude of the solids flux as the BCC in the left region. As shown in Figure 8, their flow states, including both bubble size and flow directions, are very similar. In the right region of the ACC, the fluctuating frequency of solids flux is smaller than that of the left region, as shown in Figure 8(b). The bubble size is also smaller than that of in the BCC in Figure 9 (a). The particles are always moving downward without any back-mixing motion. According to gas-solids spatial profiles in Figure 9, the particles are circled to ascend in the left region due to the generation and broken of bubbles. The small bubbles in the right region have a small influence to the downward movement of particles.

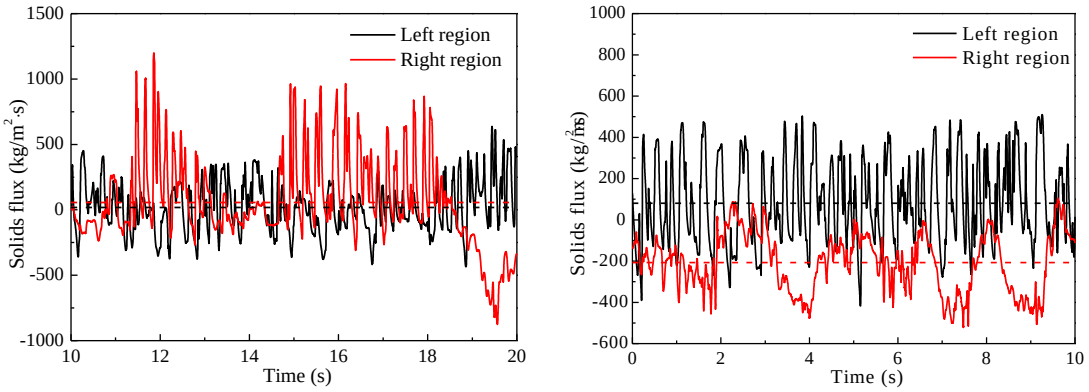

(a) BCC (b) ACC

Figure 8 Instantaneous solids fluxes in the two regions (u=0.3 m/s, r/R_w=0.8 and z=0.5)

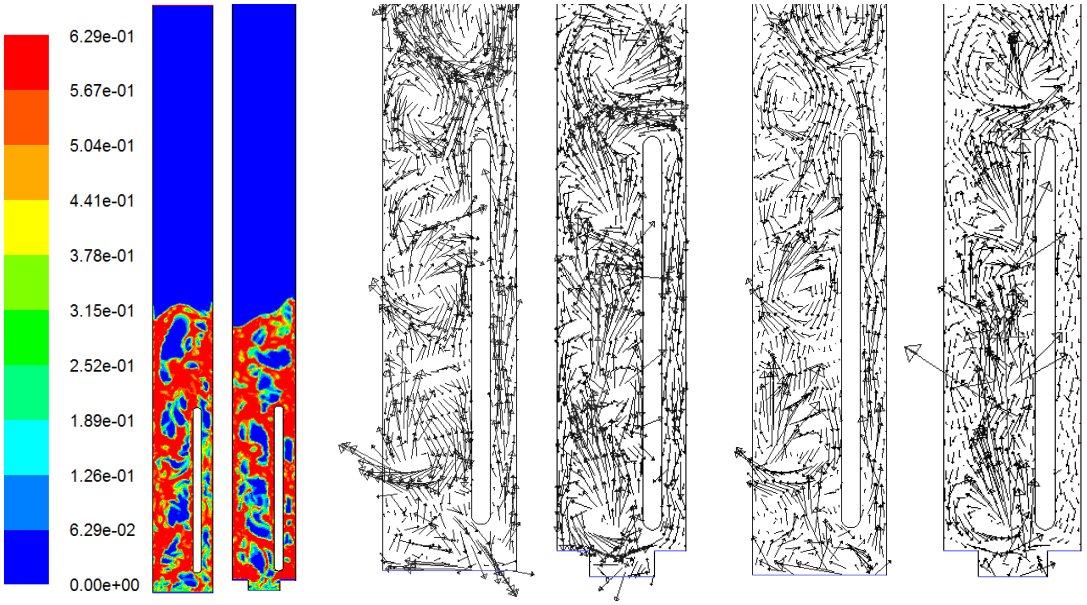

(a) Solids volume fraction (b) solids velocity (c) gas velocity

Figure 9 Gas-solids spatial profiles at a simulation time of 60 s for the representative state (u=0.3 m/s and r/R_w=0.8)

Both standard derivation and mean value of the solids flux are computed to compare the axial distributions of solids volume fraction and velocity in the two regions of BCC and ACC. The results from the BCC are shown in Figure 10. At the bottom of the heat tube (z<0.2 m), both solids volume fraction and velocity are smaller than those in the upper region, resulting from the combined impact of a small distance from the distributor and a turbulent flow across the heat tube. In both sides of the heat tube, there is small difference in the solids volume fraction. However, a slightly bigger solids velocity occurs in the right region due to the wall effect, which causes the particles to have an instantaneous and rapid motion. The right region has a larger standard derivation in solids volume fraction and velocity than those of the left region, which indicates the inferior flow stability in the right region due to the wall effect. The flow state leads to a uniform axial distribution of heat transfer coefficient in the BCC, as shown in Figure 12. At the top of the heat tube (i.e., z>0.9 m), the solids velocity becomes smaller and the solids volume fraction increases, mainly due to the increase of the flow area.

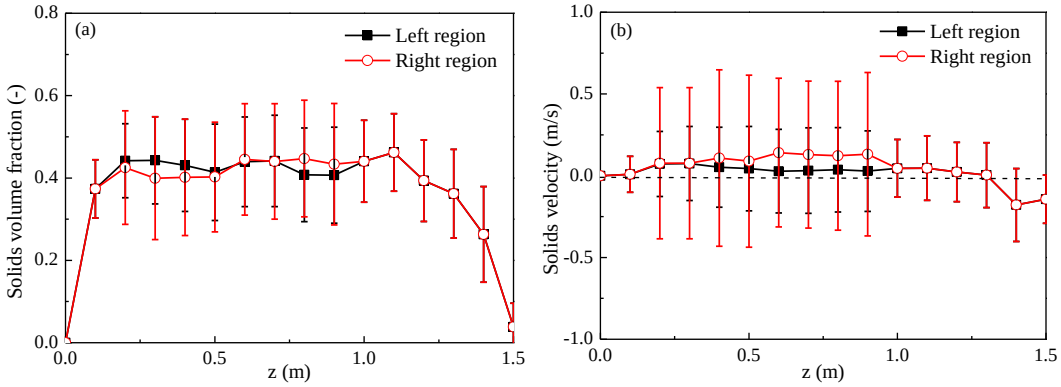

(a) Solids volume fraction (b) Solids velocity

Figure 10 Comparison of solids volume fraction and velocity in two regions of heat tube (BCC) (u=0.3 m/s and r/R_w=0.8)

Although there is a turbulent flow, Figure 11 shows that the solids volume fraction at the tube bottom is bigger than the upper region of the ACC. The velocity of solids is also smaller. This further indicates the radial movement of particles at the tube bottom. At 0.2 m ≤ z < 0.6 m, the solids volume fraction in the right region is bigger and their difference decreases with increasing axial height, which is the driving force of internal circulation. The solids velocity has almost no change in the whole left region. In the right region, the solids velocity has no change at 0.2 m ≤ z < 0.5 m, resulting from bigger solids volume fraction, which limits the solids movement. Rapid decrease of the particle velocity is observed as the particles reach z~0.5, but subsequently remains a constant value at the regions of 0.6 m ≤ z ≤0.9 m. The standard derivations for both solids fraction and solids velocity in the right region are bigger than the left region, which indicates that there is an inferior steady flow in the right region, despite of the downward movement of particles. Such observations are consistent with our experimental determined heat transfer coefficients [13], Figure 12. Comparing to the BCC, larger heat transfer coefficients are observed in the ACC, possibly due to increased particle renewal frequency, and the enhancement decrease with increasing axial height. Such a trend is attributed to the difference of solids volume fraction at 0.2 m ≤ z < 0.5 m, which enhances the internal circulation of particles.

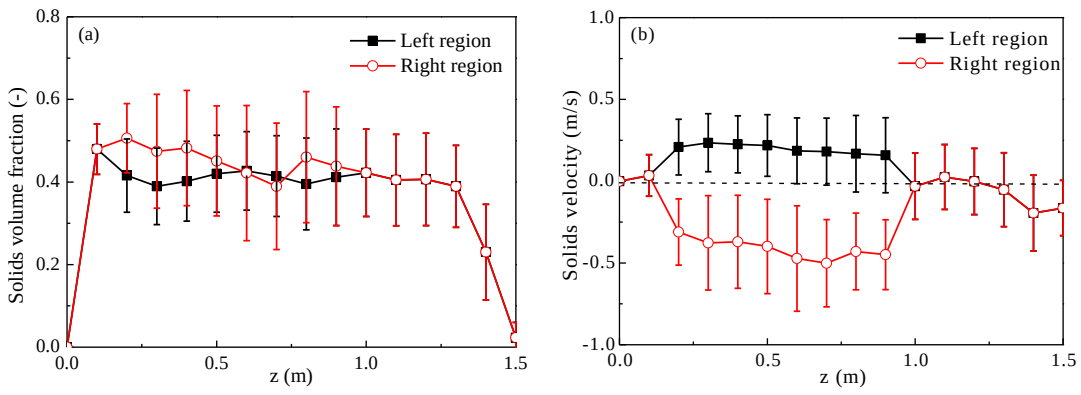

(a) Solids volume fraction (b) Solids velocity

Figure 11 Comparison of solids volume fraction and velocity in two regions of heat tube (ACC) (u=0.3 m/s and r/R_w=0.8)

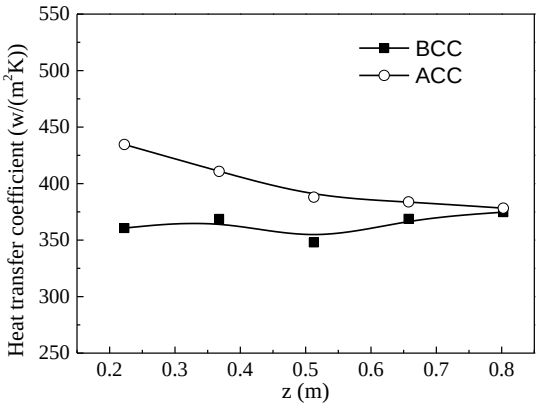

Figure 12 Comparison of heat transfer coefficient in axial direction [13]

4.3 Bed expansion ratio

Figure 13 compares the bed expansion heights of the BCC and ACC. The simulated axial profiles of radial-averaged solids volume fraction are in good agreement with the experimental values at different superficial gas velocities. In both catalyst coolers, the solids volume fractions decrease and the bed heights increase with increasing gas velocity. However, the ACC has a bigger solids volume fraction than the BCC under the same operation conditions, hence a smaller expansion height. The difference is due to the bigger solids volume fraction in the right region of ACC, as shown in Figure 11(a).

Such results reveal that the solids internal circulation can improve the solid profiles by increasing the solid volume fractions and decreasing the residence time of particles on the heat tube by increasing the solids velocity. As mentioned in a previous study [57], both factors are beneficial to increase the heat transfer coefficient. The ACC has combined features of both up- and down-flow catalyst coolers.

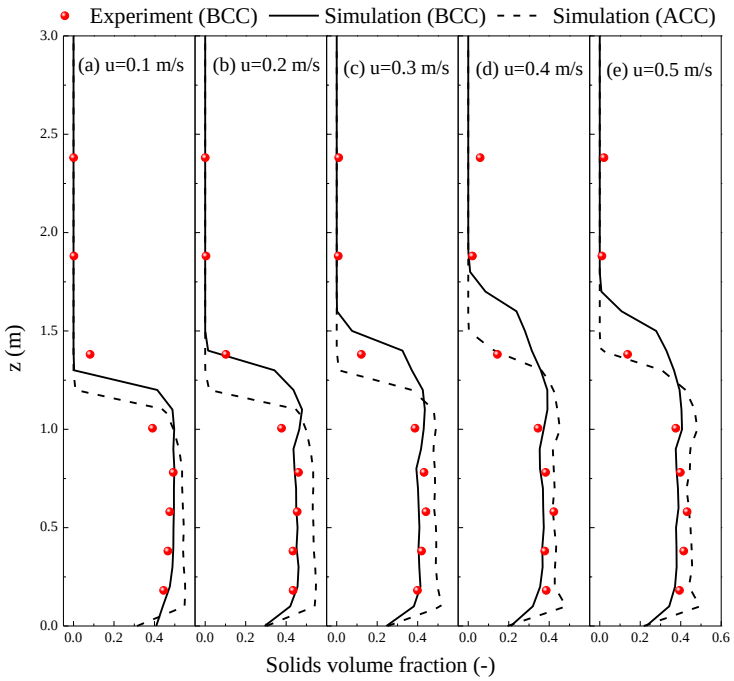

Figure 13 Comparison of axial profiles of radial-averaged solids volume fraction in two catalyst coolers (r/R_w=0.8)

4.4 Effect of operation conditions on the internal circulation

4.4.1 Gas velocity from centre distributor

Figure 14 describes the effect of gas velocity from the centre distributor on the solids volume fraction, velocity and flux in both sides of the heat tube. At a low gas velocity of 0.1 m/s, the right region has smaller solids volume fraction, bigger solids velocity and flux than the left region. The bigger standard derivation in the right region indicates an unstable flow state. The internal circulation is not formed due to the uniform gas distribution at u=0.1 m/s. At u=0.2 m/s, the solids volume fractions, velocities and fluxes are close in both regions of the ACC. The internal circulation rate of particles increases with increasing gas velocity from the center distributor. Although both the solids volume fractions decrease in two regions, their difference increases with increasing gas velocity. The standard derivations show that both solids volume fraction and velocity have bigger fluctuations in the right region. At u>0.2 m/s, the gas velocity in the centre region has no effect on the solids flux. Hence, it is necessary to have the ratio of gas velocity from two distributors $u_1'/u_2' > 12$ in order to form a stable internal circulation, which is in good agreement with experimental results [13].

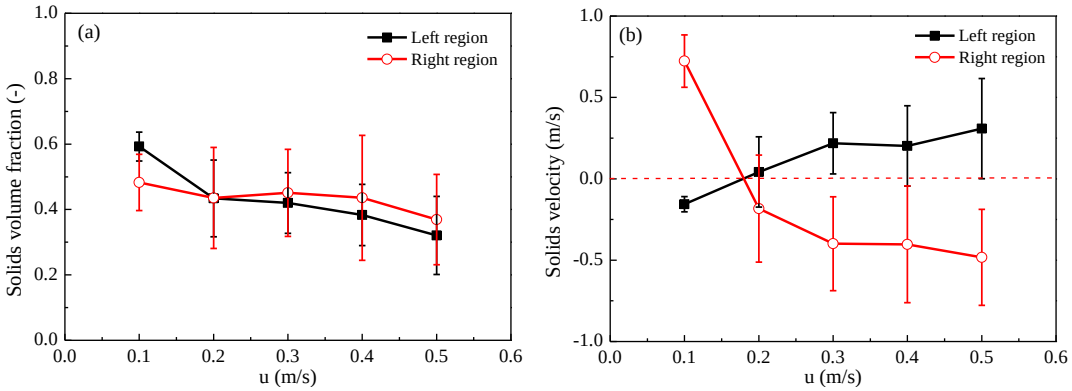

(a) Solids volume fraction (b) Solids velocity

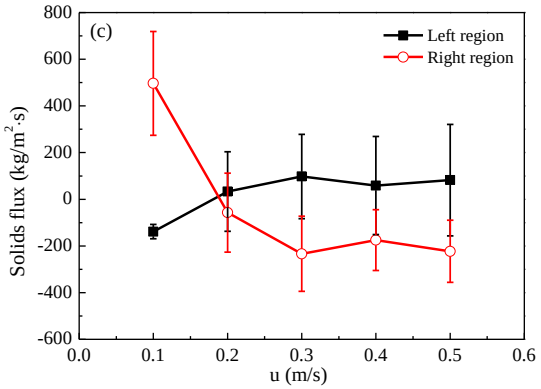

(c) Solids flux

Figure 14 Effect of the superficial gas velocity on flow performance in two regions of the heat tube in ACC (r/R_w=0.8, z=0.5 m)

4.4.2 Radial position of heat tube

Figure 15 quantitatively compares the solids volume fraction, velocity, and flux in both sides of the heat tube at different radial positions of the heat tube. Bigger standard derivations indicate strong back-mixing motion at r/R_w = 0.0 and 0.3. Although there are some differences in the solids velocity and flux, there is not a real circulation formed as shown in Figures 5(a) and 6(a). At $r/R_w \geq 0.3$, the solids volume fractions in the right region are bigger than the left region. Their difference decreases with increasing the radial position of heat tube. Both solids volume fraction and velocity decrease as the heat tube moves to the bed wall in the left region. In the right region, they first have no change and then decrease. The cut-off point is at r/R_w = 0.8. The solids internal circulation is directly influenced by the solids flux in two sides of heat tube. Therefore, the internal circulation decreases with heat tube closing to the wall due to reducing the flow area in the right region. In the left region, the back-mixing motion will get strong. Combining Figures 5 and 6, it suggests that an optimal position of heat tube is at $0.6 \leq r/R_w \leq 0.8$, where a stable internal circulation with a large circulation rate indicates a very good heat transfer between the bed and

tube wall. Such simulated results are in good agreement with our experimental values [13].

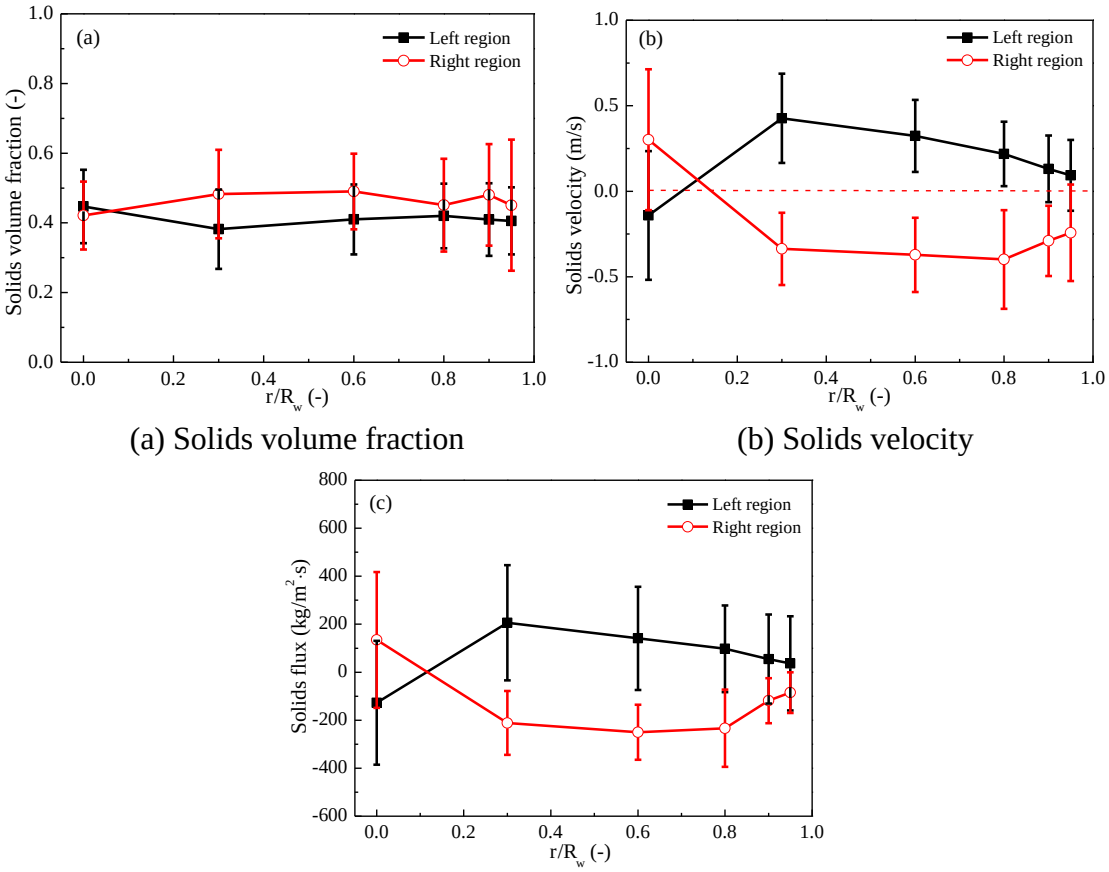

(a) Solids volume fraction (b) Solids velocity

(c) Solids flux

Figure 15 Effect of the radial position of heat tube on flow performance in two regions of heat tube in ACC (u=0.3 m/s, z=0.5 m)

5. CONCLUSION

Gas-solids flow dynamics of the BCC and ACC are numerically investigated based on the two-fluid model with a modified Gidaspow drag model. A good agreement is obtained between the numerical simulation and experimental results, and the main points can be summarized:

(1) Due to different distributor, two catalyst coolers present different fluidizing state. Two sides of heat tube have same volume fraction and flow direction, similar fluctuation frequency, which indicate a typical characteristics of bubbling bed in the BCC. In the left region of the ACC, there are a bigger rising velocity of solids and a smaller solids volume fraction than those in the BCC, which is a bubbling fluidization with a high velocity. In its right region, particles with bigger volume fraction move downward with a small velocity, which is a bubbling fluidization with low velocity. Therefore, the ACC has a combined

hydrodynamics of up- and down-flow catalyst coolers, i.e., bigger solids volume fraction and smaller resident time of particle in the view of the bed, which are helpful to increase the bed-to-tube heat transfer coefficient.

(2) At same operation condition, the ACC has a smaller expansion ratio, which is attributed to movement downward of particles with bigger solids volume fraction in the right region.

(3) In the ACC, there is an internal circulation due to the difference of gas velocity in two sides of heat tube. When fixing the position of the heat tube, solids volume fractions decrease and solids velocities increase in two regions with increasing gas velocity from plate distributor. Moreover, a bigger increase of solids velocity is obtained in the right region. The internal circulation keeps a constant at $u>0.2$ m/s. At constant superficial gas velocity, solids volume fraction is influenced by the radial position of heat tube. However, both solids velocity and internal circulation decrease with heat tube closing to bed wall.

(4) The internal circulation can be kept to need the certain operation conditions, i.e., $u >0.2$ m/s, $r/R_w>0.3$.

(5) In the solid wall boundary condition of Johnson and Jackson, the specularity coefficient has significant effect on the locally instantaneous solids volume fraction. However, the average solids volume fraction is not almost influenced by the specularity coefficient. The specularity coefficient 0.3 is a reliable choice in order to ensure the agreement between simulated and experimental values.

Nomenclature

A flow area, m

C_D drag coefficient

d_p diameter of particle, m

d_p^* effective particle diameter, m

e restitution coefficient

e_w wall coefficient of restitution

g_i acceleration due to gravity, m/s^2

g_0 radial distribution function

H_0 Static bed height, m

p pressure, Pa

Re_p Reynolds number

R radius of fluidized bed, m

R_w maximum radial position that the heat transfer tube can reach, i.e., R- r_t, m

r_t the radius of the heat tube, m

t time, s

u velocity, m/s

u_t terminal velocity, m/s

u_t^* experimental terminal velocity, m/s
x coordinate
z distance from the plate distributor, m

Greek letters
β interphase momentum exchange coefficient, kg/(m^3·s)
γ collisional dissipation of energy fluctuation, kg/(m^3·s)
ε volume fraction
ε_o initial solids volume fraction
ξ_p solid bulk viscosity, Pa·s
Θ granular temperature, m^2/s^2
μ viscosity, Pa·s
μ_p solid phase shear viscosity, Pa·s
ρ density, kg/m^3
φ Specularity coefficient
τ stress tensor, Pa
Γ_Θ diffusion coefficient for the energy fluctuation, kg/(m·s)

Subscripts
1 plate distributor in ACC
2 ring distributor in ACC
i, j, k direction coordinate
g gas phase
max maximum
p particulate phase
mf Minimum fluidization

Acknowledgments

References
[1] T.Y. Chan, D.S. Soni, F. Zhang, Advances in a catalyst cooler technology, Petrol. Technol. Q. Autumn 87 (1999) 83-84.
[2] R. Pillai, P.K. Niccum, FCC catalyst coolers open window to increased propylene, in: Grace Davison FCC Conference, Munich, 2011.
[3] R.A. Lengemann, FCC process with dual function catalyst cooling. US Pat. US5800697, 1998.
[4] D.A. Lomas, G.J. Thompson, Fluid particle cooling process and apparatus. US Pat. US4434245A, 1984.
[5] S.Z. Fu, J.Z. Zhang, D.B. Geng, Failure analysis and precaution measures for heat exchange tube bundles in RFCC catalyst cooler. Chem. Eng. Equip. 1 (2011) 103-107 (in Chinese).

[6] Y.Z. Gu, Q.S. Li, L. Li, Analysis of thermal stress of catalyst cooler finned tubes and optimization of construction. Pet. Ref. Eng. 39 (2009) 36-41 (in Chinese).
[7] L.R. Anderson, H.S. Kim, T.G. Park, H.J. Ryu, S.J. Jung, Operations adjustments can better catalyst-cooler operations. Oil Gas J. 97 (1999) 53-56.
[8] Y.J. Zhao, F. Bai. Modification of heat exchanger 800,000 tons/year catalytic cracking device. Guangzhou Chem. Industry. 42 (12) (2014)175-178(in Chinese).
[9] J.G. Yi. Failure analysis and improvement of heat removing tube of external heat collector, Pressure vessel. 28 (4) (2011) 52-56 (in Chinese).
[10] X.F. Zhou, Treatment and cause analysis of heat tube leak in external catalyst cooler of catalytic cracking unit, Petrol. & chem. Equip. 6(2012) 64-66, 70(in Chinese).
[11] H. Huang, Failure analysis of Refractory lining in connection pipelines of catalyst cooler, Corrosion & protection in petrochemical industry. 30(3) (2013) 48-50 (in Chinese).
[12] X.Y. Yao, F.W. Sun, Y.M. Zhang, C.X. Lu. Experimental validation of a new heat transfer intensification method for FCC external catalyst coolers, Chem. Eng. Process. 75(2014)19-30.
[13] X.Y. Yao, Y.M. Zhang, C.X. Lu, H. Xiao, Investigation of the Heat Transfer Intensification Mechanism for a New Fluidized Catalyst Cooler, AIChE J. 61(8) (2015) 2415- 2427.
[14] B.J. Alappat, V.C. Rane, Solid circulation rate in recirculating fluidized bed, J. Energy Eng. 127(2)(2001) 51-67.
[15] M. Liu, J. Xie, C. Lu, Z. Wang. Theoretical analysis of hydrodynamics in novel gas-solid annulus-spargered airlift loop reactor, J. Chem. Ind. Eng. (China). 59(9) (2008) 2198-2205 (in Chinese).
[16] M. Liu, Z. Shen, L. Yang, C. Lu, Microscale two-phase flow structure in a modified gas-solid fluidized bed, Ind. Eng. Chem. Res. 53 (2014) 13475-13487
[17] C. Yan, C. Lu, Y. Zhang, D. Wang, M. Liu, Profiles of solid fraction and heterogeneous phase structure in a gas-solid airlift loop reactor, Chem. Eng. Sci. 65 (2010) 2707-2726.
[18] C. Yan, C. Lu, Y. Fan, R. Cao, Y. Liu, Experiments and simulations of gas–solid flow in an airlift loop reactor, Particuology, 9 (2011) 130-138.
[19] C. Yan, C. Lu, Y. Liu, R. Cao, M. Shi, Hydrodynamics in airlift loop section of petroleum coke combustor, Powder Technol. 192 (2009) 143-151.
[20] M Liu, J. Xie, Z Meng, C. Lu, Hydrodynamic characteristics and mixing characteristics of a new type particle mixer, J. Chem. Eng. Japan. 48 (2015) 564-574.
[21] L. Zhu, Y. Fan, C. Lu, Mixing of cold and hot particles in a pre-lifting scheme with two strands of catalyst inlets for FCC riser, Powder Technol. 268 (2014) 126-138.
[22] J. Wang, M.A. van der Hoef, J.A.M. Kuipers, CFD study of the minimum bubbling velocity of Geldart A particles in gas-fluidized beds, Chem. Eng. Sci. 65 (2010) 3772-3785.
[23] B. Lu, N. Zhang, W. Wang, J. Li, J.H. Chiu, S.G. Kang, 3-D full-loop simulation

of an industrial-scale circulating fluidized-bed boiler, AIChE J. 59 (2013) 1108-1117.
[24] Y. Guan, J. Chang, K. Zhang, B. Wang, Q. Sun, Three-dimensional CFD simulation of hydrodynamics in an interconnected fluidized bed for chemical looping combustion, Powder Technol. 268 (2014) 316-328.
[25] J.A.M. Kuipers, W. Prins, W.P.M. Van Swaaij, Numerical calculation of wall-to-bed heat-transfer coefficients in gas-fluidized beds, AIChE Journal, 38 (1992) 1079-1091.
[26] D.J. Patil, J. Smit, M. van Sint Annaland, J.A.M. Kuipers, Wall-to-bed heat transfer in gas–solid bubbling fluidized beds, AIChE Journal, 52 (2006) 58-74.
[27] R. Yusuf, B. Halvorsen, M.C. Melaaen, An experimental and computational study of wall to bed heat transfer in a bubbling gas–solid fluidized bed, International Journal of Multiphase Flow, 42 (2012) 9-23.
[28] Legawiec, B., Ziolkowski, D., 1994. Structure, voidage, and effective thermal conductivity of solids within near-wall region of beds packed with spherical pellets in tubes. Chem. Eng. Sci. 49, 2513–2520.
[29] Zehner, P., Schluender, E.U., 1970. Warmeleitfaehig eit von schuettungen bei maessignen temperaturen. Chem. Eng. Technol. 42, 933–941.
[30] L.M. Armstrong, S. Gu, K.H. Luo, Study of wall-to-bed heat transfer in a bubbling fluidised bed using the kinetic theory of granular flow, International Journal of Heat and Mass Transfer, 53 (2010) 4949-4959.
[31] N.H. Dong, L.M. Armstrong, S. Gu, K.H. Luo, Effect of tube shape on the hydrodynamics and tube-to-bed heat transfer in fluidized beds, Applied Thermal Engineering, 60 (2013) 472-479.
[32] R. Yusuf, B. Halvorsen, M.C. Melaaen, Eulerian–Eulerian simulation of heat transfer between a gas–solid fluidized bed and an immersed tube-bank with horizontal tubes, Chemical Engineering Science, 66 (2011) 1550-1564.
[33] G. Ferschneider, P. Mege, Eulerian Simulation of Dense Phase Fluidized Beds, Rev. Inst. Fr. Pét., 51 (1996) 301-307.
[34] B.G.M. van Wachem, J.C. Schouten, C.M. van den Bleek, R. Krishna, J.L. Sinclair, Comparative analysis of CFD models of dense gas–solid systems, AIChE Journal, 47 (2001) 1035-1051.
[35] T. McKeen, T. Pugsley, Simulation and experimental validation of a freely bubbling bed of FCC catalyst, Powder Technol. 129 (2003) 139-152.
[36] P. Lettieri, D. Newton, J.G. Yates, Homogeneous bed expansion of FCC catalysts, influence of temperature on the parameters of the Richardson–Zaki equation, Powder Technol. 123 (2002) 221-231.
[37] J. Gao, J. Chang, C. Xu, X. Lan, Y. Yang, CFD simulation of gas solid flow in FCC strippers, Chemical Engineering Science, 63 (2008) 1827-1841.
[38] J. Gao, X. Lan, Y. Fan, J. Chang, G. Wang, C. Lu, C. Xu, CFD modeling and validation of the turbulent fluidized bed of FCC particles, AIChE J. 55 (2009) 1680-1694.
[39] Y. Liu, X. Lan, C. Xu, G. Wang, J. Gao, CFD simulation of gas and solids mixing in FCC strippers, AIChE J.58 (2012) 1119-1132.

[40] J. Wang, A Review of Eulerian Simulation of Geldart A Particles in Gas-Fluidized Beds. Ind. Eng. Chem. Res. 48 (2009) 5567-5577.
[41] P. Johnson, R. Jackson, Frictional-collisional constitutive relations for granular materials, with application to plane shearing, J. Fluid Mech. 176 (1987) 67–93.
[42] S. Benyahia, M. Syamlal, T.J. O'Brien, Evaluation of boundary conditions used to model dilute, turbulent gas/solids flows in a pipe. Powder Technol. 156 (2005) 62-72.
[43] T. Li, J. Grace, X. Bi, Study of wall boundary condition in numerical simulations of bubbling fluidized beds, Powder Technology, 203 (2010) 447-457.
[44] H. Zhong, J. Gao, C. Xu, X. Lan, CFD modeling the hydrodynamics of binary particle mixtures in bubbling fluidized beds: Effect of wall boundary condition, Powder Technology, 230 (2012) 232-240.
[45] X. Lan, C. Xu, J. Gao, M. Al-Dahhan, Influence of solid-phase wall boundary condition on CFD simulation of spouted beds, Chemical Engineering Science, 69 (2012) 419-430.
[46] L. Kong, C. Zhang, J. Zhu, Evaluation of the effect of wall boundary conditions on numerical simulations of circulating fluidized beds, Particuology, 13 (2014) 114-123.
[47] M. Upadhyay, J.-H. Park, CFD simulation via conventional Two-Fluid Model of a circulating fluidized bed riser: Influence of models and model parameters on hydrodynamic behavior, Powder Technology, 272 (2015) 260-268.
[48] C. Loha, H. Chattopadhyay, P.K. Chatterjee, Euler-Euler CFD modeling of fluidized bed: Influence of specularity coefficient on hydrodynamic behavior, Particuology, 11 (2013) 673-680.
[49] T. Li, Y. Zhang, J.R. Grace, X. Bi, Numerical investigation of gas mixing in gas-solid fluidized beds, AIChE J, 56 (2010) 2280-2296.
[50] J.R. Grace, T. Li, Complementarity of CFD, experimentation and reactor models for solving challenging fluidization problems, Particuology 8 (2010) 498–500.
[51] M.T. Shah, R.P. Utikar, V.K. Pareek,M.O. Tade, G.M. Evans, Effect of closuremodels on Eulerian-Eulerian gas-solid flow predictions in riser, Powder Technol. 269 (2015) 247-258.
[52] A. Bahramian, M. Olazar, G. Ahmadi, Effect of slip boundary conditions on the simulation of microparticle velocity fields in a conical fluidized bed, AIChE J. 59 (2013) 4502–4518.
[53] S. Benyahia, M. Syamlal, T.J. O'Brien, Study of the ability of multiphase continuum models to predict core-annulus flow, AIChE J. 2007, 53(10): 2549-2568.
[54] L.M. Armstrong, S. Gu, K.H. Luo, The influence of multiple tubes on the tube-to-bed heat transfer in a fluidised bed, Int. J. Multiphase Flow, 36 (2010) 916-929.
[55] A. Bakshi, C. Altantzis, R.B. Bates, A.F. Ghoniem, Eulerian–Eulerian simulation of dense solid–gas cylindrical fluidized beds: Impact of wall boundary condition and drag model on fluidization, Powder Technology, 277 (2015) 47-62.
[56] B. Lu, W. Wang, J. Li, Eulerian simulation of gas–solid flows with particles of

Geldart groups A, B and D using EMMS-based meso-scale model, Chem. Eng. Sci. 66 (2011) 4624-4635.

[57] X. Yao, Y. Zhang, C. Lu, X. Han, Systematic study on heat transfer and surface hydrodynamics of a vertical heat tube in a fluidized bed of FCC particles, AIChE J. 61 (2015) 68-83.